Surfaces and Interfaces 56 (2025) 105625

Contents lists available at ScienceDirect

Surfaces and Interfaces

journal homepage: www.sciencedirect.com/journal/surfaces-and-interfaces

New synthesis of 2D halide perovskites assisted by the Langmuir-Schaefer methodology

Rania Daoudi [a], David Durán [a], David López-Díaz [a], Ana Pérez-Rodríguez [b], Maha Labani [b], M. Dolores Merchán [a,b,c], M. Mercedes Velázquez [a,b,c,*]

[a] Departamento de Química Física, Facultad de Ciencias Químicas, Universidad de Salamanca E37008, Salamanca, España
[b] Grupo de Nanotecnología, Universidad de Salamanca E37008, Salamanca, España
[c] Laboratorio de Nanoelectrónica and Nanomateriales, USAL-NANOLAB, Universidad de Salamanca E37008, Salamanca, España

ARTICLE INFO

Keywords:
Synthesis of 2D bromide perovskites at the interface
Langmuir-Blodgett films
Langmuir-Schaefer films

ABSTRACT

Perovskites have emerged as a promising component of photovoltaic cells due to their high efficiency and compatibility with various fabrication processes. In the last years, many efforts have been made to eliminate the structural defects which reduce their quantum efficiency. Surface passivation by organic molecules, two-dimensional (2D) halide perovskites, has provided the best results. However, the development of synthesis to obtain high quality materials and the design of solid transfer processes that lead to highly ordered layered films, necessary for the preparation of devices, remains a challenge. Therefore, we report for the first time a new synthesis at the interface assisted by the Langmuir-Schaefer methodology (LS) to obtain 2D lead perovskites passivated with the surfactant octadecylammonium bromide (ODAB). In our synthesis, the ammonium salt was spread on a subphase containing lead and potassium bromides, and then, the monolayer was compressed until achieve a dense monolayer of ODAB and layered perovskite. The monolayer was then transferred to solids using the Langmuir-Blodgett (LB) and Langmuir-Schaefer (LS) methodologies. The structural characterization of the films was conducted by absorption UV–vis and Raman spectroscopies, X-Ray diffraction (XRD) and scanning electronic (SEM) and atomic force (AFM) microscopies. Our results demonstrate that the highest coverage was achieved by the LS method. Extensive structural analysis has shown that perovskites contain only a layer of inorganic material between bilayers of the organic material. 2D perovskites prepared by this methodology show higher crystallinity than those prepared by other syntheses.

1. Introduction

Metal halide perovskites (MHPs) have attracted a great interest in recent years due to their excellent properties such as absorption of light in a wide range of wavelengths, easy bandgap modification, high electronic mobility and high capacity to absorb light and convert it into useful energy [1]. All these properties make them a very attractive material as a component of photodetectors [2,3], ionizing radiation detectors [4], photovoltaic cells [5–9] or light emitting diodes (LEDs) [10,11].

The building block of halide perovskites is the metal halide octahedral $[BX_6]^{4-}$ (B=Pb^{2+}or Sn^{2+}, and X is a halogen), which can be arranged in three-dimensional (3D), two-dimensional, (2D), one-dimensional (1D) or even zero-dimensional (0D) structures [12]. Three-dimensional metal halide perovskites, ABX_3, where A represents an organic ammonium cation, exhibit tunable optical properties and high fluorescence quantum yields [13], but their high instability limits their applications [14]. This instability is due to structural defects such as lattice defects and dangling bonds which reduce the quantum efficiency [15]. In addition, ionic migration leads to charge accumulation at the surface, which creates barriers for charge injection and degrades the structure of the material [15]. Surface passivation by shell molecules has been proposed to improve perovskite stability [16,17]. Although a large number of molecules have been proposed for passivation, theoretical [18] and experimental [19,20] results indicate that quaternary amines promote strong passivation effects. These ionic molecules stabilize the material by formation of hydrogen bonds with the halide anions of the perovskite, suppressing their migration and passivating the interstitial

* Corresponding author: Departamento de Química Física, Facultad de Ciencias Químicas, Plaza de los caídos s/n. Universidad de Salamanca E37008, Salamanca, Spain.
E-mail address: mvsal@usal.es (M.M. Velázquez).

https://doi.org/10.1016/j.surfin.2024.105625
Received 23 August 2024; Received in revised form 11 December 2024; Accepted 12 December 2024
Available online 12 December 2024

halide [21]. Accordingly, two-dimensional metal halide perovskites described by the following formula $(RNH_3)_2B_nX_{3n+1}$, where RNH_3 is a large organic ammonium cation, show improved stability due to the protection of the organic layer. In the formula, n represents the number of monolayer metal halide sheets in the layered structures, and depending on its value, the structure can be described as [22]: 2D ($n = 1$), quasi-2D ($n = 2$–5) and ($n > 5$) 3D perovskites.

In the case of 2D metal halide perovskites, their structure contains just one inorganic semiconductor layer of two-dimensional octahedral BX_6 that shares corners while the dielectric organic layers of RNH_3 are stacked alternately [23]. Compared with the polycrystalline films ($n \geq 2$), they contain less surface defects, exhibit higher crystallinity, stability and device performance [24,25]. However, despite extensive research efforts in recent years resulting in improved photoluminescence quantum yield, efficient electroluminescence [26,27] and power conversion efficiency up to 29.5 % [28], the reached quality is not sufficient for device applications; therefore, the development of high-quality materials synthesis routes, and the design of solid-state transfer processes that achieve highly ordered layered films with minimal number of defects is currently the subject of extensive research.

The most universal method to synthesize 2D metal halide perovskites uses a slow cooling crystallization process [26] in which the precursors are dissolved in an acidic solution at a temperature high enough to dissolve them, followed by slow cooling, typically several days, until the 2D perovskites are obtained. However, this method often leads to quasi-2D or 3D perovskites [27] with $n \geq 2$. Another way to obtain 2D perovskite crystals is to employ a mixture of solvents, including good, moderate, and anti-solvents, to create atomically thin uniform nanocrystals by a quick evaporation [28]. Other method involves mechanical exfoliation of bulk materials to prepare single crystals with n values between 1 and 4 [29]. All these methods have their advantages and disadvantages. Thus, the direct synthesis of nanocrystals produces uniform sizes and shapes, while the exfoliation method leads to random shapes and thicknesses [30]. However, direct synthesis is limited by short crystallization growth times, resulting in low crystal quality. Besides, the synthesis in bulk uses conventional transfer techniques as spin coating, and dipping or drop casting [31] which often lead to coffee ring effect [32] due to uncontrolled capillary flow and dewetting processes during solvent evaporation [33,34]. This effect causes inhomogeneous composition and/or phase segregation in large surface films, which deteriorates the quality of the devices. Therefore, to obtain high-quality 2D perovskites, it is necessary to develop new manufacturing routes [32]. We believe that the synthesis at interfaces could be a good alternative, because the strong asymmetry in the molecular interactions at the interface can significantly influence the orientation of molecules as well as the rate of chemical reactions [35]. Furthermore, the interfacial region provides a confined 2D space with high lateral mobility that allows the growth of large-area of 2D structures [36].

Recently, a synthesis at the interface by the Langmuir-Blodgett method (LB), has been used to construct lead layered perovskites [37–39]. The LB technique has been widely used for synthesis at interfaces and is based on the transfer process of material from the air--water interface, Langmuir monolayer, to a solid substrate by vertical dipping of the solid in the Langmuir monolayer [40–42]. The technique allows continuous variation of the density, packing and arrangement of the material by compressing or expanding the film using two barriers. Therefore, it allows precise control of the film structure at the molecular level, offering the possibility of adjusting its properties [33,34,43].

In the case of the synthesis of perovskites, the procedure consisted of preparing 2D perovskites in a Langmuir monolayer using a water-insoluble organic cation, typically docosylamonium bromide [38,39] or π-conjugated materials such as phenylenevinylene oligomers, dithienylethene derivatives or polyfluorene [44] spread on the aqueous subphase containing the lead salt and then starting the compression of the monolayer. Reflection UV–vis spectra of the monolayer at different surface pressure values show that the formation of layered-perovskite structure starts at the edge of the plateau region of the isotherm and continues after further compression [38,45]. The layered-perovskite was formed above the plateau and transferred by LB from the air-water interface to different solids such as mica [38] or quartz [39]. However, to achieve high coverage, it was necessary to transfer several layers of perovskites (typically from 10 to 20) [37,44]. We believe that it is possible to improve both the molecular order and the film coverage, using the Langmuir-Schaefer technique (LS). In this methodology the solid touches the Langmuir monolayer horizontally [46] to construct monolayers or multilayers by repeating the touching and lifting procedure. This method gives better results than LB for rigid monolayers [42] and was used for low dimensional nanomaterials [47,48]. Besides, since the substrate is not immersed in the aqueous subphase, undesirable inhomogeneities and segregation processes due to the solvent evaporation are minimized. In addition, in the case of LS multilayers, it is possible to modify the orientation of the different layers to obtain different patterns without a defined template [49,50]. We think that the LS technique could provide the enormous advantage of being able to tune the structure and properties of 2D perovskites in a straightforward way, simply by modifying the organic molecule spread at the interface or the salt dissolved in the aqueous subphase. In addition, the LS methodology is a scalable procedure which can be used to fabricate large-area monolayer films [51].

Based on this framework, the aim of this research is to explore the ability of the LS methodology to construct highly crystalline 2D halide perovskite films. With this aim in mind, we prepare two-dimensional lead halide perovskites using Langmuir films of the surfactant octadecylammonium bromide (ODAB) spread on an aqueous subphase of $PbBr_2$ saturated with KBr. The perovskite synthesized at the air-liquid interface are further transferred to solids by both LB and LS methodologies. We have used these two methods because we are interested in comparing the quality of films obtained by the two methodologies to confirm which of them drives to better quality films. The surfactant ODAB was chosen because it is an ammonium salt capable of suppressing the migration of halide ions from the perovskite. In addition, its molecular structure is simpler than others used in the synthesis of perovskites at the air-water interface, and forms dense and ordered perovskite monolayers, which could minimize interstitial defects and increase the crystallinity of 2D perovskites. To minimize the number of poorly coordinated Pb atoms [52], we have used aqueous subphase saturated with Br^- ions.

The work is organized as follows: firstly, we analyze the experimental conditions required to obtain dense monolayers of 2D lead perovskites. In the next section, we compare films fabricated by the LB and LS methodologies using Scanning Electron Microscopy (SEM). Since the LB drives to poor coverage compared with LS method, in the next section we analyze the structure of the 2D perovskite LS films of different layers (≤ 5) by UV–vis transmission and Raman spectroscopies. A thickness analysis was done by Atomic Force Microscopy (AFM). Finally, the quality of the LS films was analyzed in terms of crystallinity [53] using X-Ray diffraction measurements (XRD).

2. Experimental section

2.1. Materials

Octadecylamine (99 %), Hydrobromic acid (48 % w: w) and $PbBr_2$ (98 %) were supplied by Sigma Aldrich. Acetonitrile (99 %) stabilized with 6 ppm dibutylhydroxytoluene, BHT, was provided by Merck, diethyl ether (99 %) from PanReac and KBr (99.5 %) by Scharlau. All reagents were used without further purification. Hydrogen peroxide, sulfuric acid, and ammonia for cleaning the solid wafers and chloroform filtered and stabilized in ethanol for preparing the spreading solutions were provided by Sigma Aldrich. The ultrapure water used to prepare the aqueous subphase of the Langmuir trough was obtained by a combination of RiOs and Milli-Q systems from Millipore. It contains less than 5 ppb of organic matter, and its conductivity was less than 0.2 μS/cm.

The solids wafers were silicon (100) with 290 nm dry thermal SiO_2 thin film supplied by IDB Technologies Ltd (UK) and quartz from Ted Pella (USA). The solids were cleaned prior deposition. In the case of the quartz substrate, it was cleaned with acetone (PAI), ethanol (PAI) and water (Milli Q) and then maintained for 15 min in a cleaning solution (60 mL) of ammonia (25 %) and 10 mL of hydrogen peroxide (30 %) dissolved in Milli Q water at 70 °C. Finally, it was rinsed with abundant Milli Q water and dried under nitrogen stream. Silicon wafers were cleaned with acetone (PAI) and water (Milli Q). They were then kept in a solution of 70 % H_2SO_4 and 30 % H_2O_2 for 15 min, then, rinsed with water (Milli Q) and dried under a nitrogen stream.

2.2. Synthesis of octadecylammonium bromide (ODAB)

Octadecylammonium bromide was synthesized by a previously reported method [54]. Briefly, 0.5426 g of octadecyl amine were dissolved in 10 mL of acetonitrile with 0.23 mL of HBr and heated to 63 °C with stirring to give a white precipitate. The white solid was washed four times with diethyl ether [55] and then, dried under vacuum.

2.3. Experimental methods

Langmuir films were prepared on a Langmuir-Blodgett mini-trough (KSV, Finland) placed on an anti-vibration table. Pressure-area isotherms were also recorded in the Langmuir mini-trough and the surface pressure was measured with a Wilhelmy plate of Pt connected to an electrobalance. The temperature at the aqueous subphase was maintained at (25.0± 0.1) °C by flowing water through jackets at the bottom of the trough and measured with a calibrated sensor from KSV. The water temperature was controlled with a Lauda Ecoline RE-106 cryostat. For the synthesis of the organic hybrid 2D perovskites, the aqueous subphase in the Langmuir-Blodgett mini-trough contained 5.0×10^{-5} M $PbBr_2$ and 1.0 M KBr dissolved in water (Milli Q). We selected this subphase because it had previously been used to obtain Langmuir films of perovskites with docosylammonium bromide as the organic moiety, with good results [45]. The spreading solution was prepared by dissolving ODAB in chloroform by sonication for 15 min. The solution concentration was 1 mM. The spreading solution was spread drop by drop on the aqueous subphase with a micrometer Hamilton syringe with a precision of 1 μL. After the addition of a given volume of spreading solution and evaporation of chloroform, we wait until a stable value of surface pressure was reached, then, the equilibrium value was taken when this surface pressure remained constant for at least 15 min (pure water subphase) and 60 min (saline subphase), then compression was started. Perovskites synthesized at the air-water interface were then transferred to the solid wafers by vertical (Langmuir-Blodgett, LB) or horizontal (Langmuir-Schafer, LS) dipping. In the latter process, the solid substrate is placed parallel to the air-water interface and the transfer is completed by contacting the substrate with the floating monolayer using a Holder model KN 0006 from KSV. The 2D halide perovskites were transferred from the air-water interface to the solid wafers by symmetric barrier compression (5 mm/min) with the substrate into the trough by vertical (LB) and horizontal (LS) dipping at 10 mm/min. The multilayer films with 1 to 5 layers were prepared as follows: after the transfer of the first layer, the film was dried under vacuum for 15 min, and then the transfer process was repeated until the desired number of layers was obtained. Finally, the chemical structure, morphology and crystallinity of the perovskite films were analyzed by UV–vis absorption and Raman spectroscopies, Scanning Electronic Microscopy (SEM), Atomic force Microscopy (AFM) and X-ray diffraction, (XRD), respectively.

2.4. X-Ray diffraction measurements

To characterize the crystallinity of perovskite films, thin film X-ray diffraction measurements were employed. Perovskite films deposited on Si/SiO_2, and quartz were mounted on a glass plate and the diffractograms were obtained in a Bruker D8 Advance powder diffractometer (Bruker Corp., Billerica, MA, USA) using Cu Kα1,2 radiation (λ = 1.54050 Å) between 2 and 25° (2θ) with a step size and step time of 0.05° and a 2.6 s, respectively. The tube operates at 40 kV and 30 mA. To calculate the spacing of the layers (d), we use the Bragg`s law, $n\lambda = 2d \sin(\theta)$, where n is the diffraction order and θ is the angle between the reflected ray and the plane formed by the material's surface.

The crystallite size was calculated from the Sherrer equation: $L = K\lambda/\beta \cos\theta$. In the equation λ is the X-ray wavelength, β represents the line broadening at half the maximum intensity, (FWHM), θ is the Bragg angle and K represents the shape factor, typically 0.94.

2.5. UV–vis transmission spectroscopy

UV–vis transmission spectra of 3- and 5-layer perovskite films deposited on quartz were recorded in a spectrophotometer Shimadzu UV-1603 using a slit of 2 nm.

2.6. Raman spectroscopy

Spectra of perovskite films were recorded with a LabRAM HR Evolution micro-Raman spectrometer (Horiba Jobin-Yvon). The spectrometer is equipped with a solid-state laser operating at 532 nm and a 100 × objective (laser spot size ≈ 1 μm^2). The calibration was carried out by checking the Si band centered at 520.7 cm^{-1}. The spectral and spatial resolutions were 2 cm^{-1} and 0.5 μm, respectively.

2.7. Scanning electronic microscopy (SEM)

Scanning electron microscopy images were taken in a Hitachi S-3000 N microscope with an accelerating voltage of 3 kV.

2.8. Atomic force microscopy (AFM)

Atomic force microscopy (AFM) measurements were carried out using a commercial head and control unit from Nanotec Electrónica S.L. (Spain) Amplitude modulation atomic force microscopy (AM-AFM), (dynamic mode with fixed frequency) was performed at room temperature and ambient conditions. CrPt-coated Si tips in cantilevers with nominal $k = 3$ N m^{-1} from Budget Sensors were employed. All data were analyzed with the WSxM freeware.

3. Results and discussion

3.1. Synthesis of 2D organic layer perovskite assisted by the Langmuir-Schaefer methodology

Prior to the transfer process, it is essential to analyze the experimental conditions required to obtain Langmuir-Blodgett and Langmuir-Schaffer films. Since the relationship between the surface concentration of the two components, organic and inorganic materials, could have a significant impact on the structure of the films, the effect of the ODAB surface concentration on compression isotherms was investigated. Fig. 1**a** presents the isotherms of ODAB obtained after the spreading of different amounts of the surfactant on the aqueous subphase in which the concentration of Pb_2Br and KBr remains constant at 5.0×10^{-5} M of $PbBr_2$ and 1.0 M of KBr, respectively. For comparison, the isotherm of ODAB spread on pure water is also reported in Fig. 1**a**. Furthermore, we calculate the surface compression modulus value, C_s^{-1}, from numerical derivatives of the surface pressure isotherms and Eq. (1).

$$C_s^{-1} = -A\left(\frac{d\pi}{dA}\right)_T \quad (1)$$

where π represents the surface pressure and A is the molecular area of

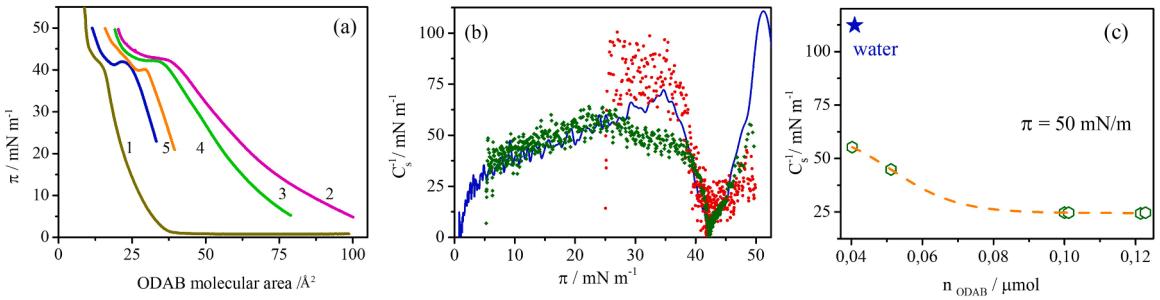

Fig. 1. (a) Surface pressure-area isotherms of ODAB spread on pure water (curve 1) and on aqueous solutions of 5.0×10^{-5} M of $PbBr_2$ mixed with 1.0 M of KBr (curves 2–5). ODAB spread on the interface was: 0.040 µmol (curves 1 and 2), 0.051 µmol (curve 3), 0.102 µmol (curve 4), and 0.123 µmol (curve 5). (b) Variation of the surface compression modulus with the surface pressure of ODAB spread on pure water (blue line) and 5.0×10^{-5} M of $PbBr_2$ and 1.0 M of KBr. ODAB spread was green diamonds (0.040 µmol) and red circles (0.121 µmol). (c) Evolution of the surface compression modulus with the ODAB amounts spread at the aqueous interface at 50 mN/m. The star represents the value of the ODAB spread on water and the dashed line is just visual guide.

ODAB. This parameter reflects the state of packing of the monolayer and is related to the elasticity in the plane [56]. Some illustrative results are plotted against the surface pressure in Fig. 1**b**.

The surface pressure-area isotherm of ODAB spread on pure water shows surface pressure values close to 0 at larger areas, above 37 $Å^2$/molecule. In this region, the compression modulus values are also close to 0. This is characteristic of molecules in a surface gas state [56]. As the molecular area decreases below 37 $Å^2$, the surface pressure increases and the compression modulus value increases until values below 50 mN/m, indicating that the monolayer is compressible and molecules are rearranged in the expanded liquid phase, (LE) [56]. If the monolayer is further compressed, the compressional modulus increases until a given value of 74 mN/m compatible with a liquid compressed phase (LC). Above this value, the compression modulus decreases and goes to a minimum at a surface pressure value of $\pi = 42$ mN/m, Fig. 1**b**. This behavior is characteristic of the transition phase that in this system corresponds to LC-S. At surface pressure values above 42 mN/m the isotherm becomes linear, and the compression modulus increases until it reaches a maximum at 112.3 mN/m. This value is compatible with the solid state [56]. The limit area estimated by extrapolating the linear part of the isotherm to the zero-surface pressure was 13 $Å^2$. This isotherm is consistent with the reported by L. Xu et al. for octadecyl ammonium chloride [57].

When the surfactant is spread on aqueous solutions of 5.0×10^{-5} M of $PbBr_2$ and 1.0 M of KBr, the isotherms become more expanded, Fig. 1**a**, and the effect has a clear dependence on the concentration of the surfactant, since when the amount of ODAB spread at the interface increases the isotherms are more compressed, although are always more expanded than the isotherm of ODAB spread on pure water. We have also analyzed the reproducibility of the isotherms. With this purpose have replicated the isotherm prepared by spreading 0.10 and 0.123 µmol of ODAB, respectively. The procedure consisted of obtaining the molecular area at the surface pressure value used for transferring perovskite films from the air-water interface to the solids (50 mN/m). The averaged values found were (15.2± 0.7) $Å^2$ and (13.5 ± 0.7) $Å^2$, respectively, where the error is calculated from the standard deviation of six measurements.

We analyze the morphology of these isotherms based on the work reported by Era et al. [38,45] concerning to the formation of lead perovskites at the air-water interface, since the morphology of our isotherms are like those obtained by the authors using docosylammonium bromide as organic water-insoluble molecule. Accordingly, at larger surface area the ODAB molecules are highly expanded, probably due to the ionic repulsions between the ammonium salt molecules and positive metal ions [45]. During the compression, a plateau region at the surface pressure of 42 mN/m appears. This plateau was also observed in previous work [38,45] and UV–vis reflection spectra of monolayers demonstrated the existence of an exciton peak around 390 nm characteristic of the layered lead-perovskite at the air–water interface, in which the octahedral lead bromide is intercalated with the ammonium salt. These layered perovskites coexist with ammonium salt molecules at the plateau, but further compression drives to the complete formation of layered perovskites [38,45]. According to these previous results, we assign the edge of the plateau to the beginning of the formation of perovskite sandwiched between ODAB molecules, whose quantity increases with further compression beyond the plateau. The appearance of the exciton peak at 390 nm in our films, see below in Fig. 4a, confirms this fact.

Our results show that the surface pressure value at the plateau remains almost constant at a value of 42 mN/m, independently on the amount of ODAB spread at the interface, as illustrated in Fig. 1**a**. Besides, they evidence that the isotherms become more compressed as the amount of ODAB spread at the interface increases, although are always more expanded than the isotherm of ODAB spread on pure water. We have also obtained the compression modulus values, since this parameter is highly sensitive to changes in the monolayer fluidity [58]. For the sake of clarity, Fig. 1**b** presents the compression modulus against surface pressure of three representative isotherms corresponding to ODAB monolayers spread on pure water and on $PbBr_2$ and KBr aqueous subphase, respectively. In the last case, the ODAB amounts spread at the interface were 0.040 µmol and 0.121 µmol, respectively. As can be seen in Fig. 1**b**, there are significant changes in the compression modulus when the ODAB molecules are spread on $PbBr_2$ and KBr aqueous subphase, although in the region of low surface pressure the compression modulus values are like those obtained in pure water. However, beyond the minimum corresponding to the phase coexistence region, the values of the compression modulus of the films that contain layered perovskites are lower than those corresponding to the surfactant spread on pure water (112.3 mN/m) and decrease when the amount of ODAB spread increases. We interpret this fact as the incorporation of perovskites between the ODAB molecules in the monolayer, which decreases the packing of the surfactant molecules. This decrease in the packing of the ODAB molecules causes a decrease in the compression modulus observed in Fig. 1**b**. This behavior has been previously reported for surfactant monolayers in which nanoparticles are incorporated [59].

Due to our interest in transferring dense perovskite monolayers, we have selected monolayers at surface pressure higher than the value corresponding to the plateau. Besides, since we want obtained higher packing monolayers, we have transferred monolayers in which the area of the ODBA molecules was close to the limit area of ODAB at the solid state (13 $Å^2$). This condition was achieved for monolayers fabricated with 0.123 µmol of ODAB at the surface pressure of 50 mN/m, (13.5 ± 0.7) $Å^2$. To confirm if these experimental conditions are the most adequate to transfer monolayers saturated of perovskites, we have analyzed in Fig. 1**c** the dependence of the compression modulus value with the concentration of surfactant spread at the interface. The results

in Fig. 1**c** show that the compression modulus decreases with the amount of ODAB spread at the interface until it reaches a value of 0.10 μmol of ODAB in which the compression modulus remains constant. This behavior indicates that at least 0.10 μmol of ODAB are needed to saturate the interface with layered perovskites for the $PbBr_2$ concentration used in the work, therefore, to build LB and LS perovskite films we spread 0.12 μmol of ODAB.

3.2. *Structural characterization of 2D organic perovskites*

In the next stage of the work, we have transferred the organic-layered perovskites at 50 mN/m from the air-liquid interface to the silicon wafer using both the Langmuir-Blodgett and Langmuir-Schaefer methodologies. We have selected this solid substrate because the silicon/perovskite tandem has been proposed as a promising candidate to achieve power conversion efficiencies above 30 % at a reasonable cost [60]. The morphology of these films was analyzed by SEM, Fig. 2.

As Figs. 2**a** and Fig. 2**b** illustrate, the coverage obtained using the LS methodology is significantly higher than that achieved with LB. In any case, the coverage of one layer LS film must also be improved by transferring a greater number of layers. Figs. 2**c and** 2**e** show images of films containing 3 and 5 layers, respectively. They illustrate the significant increase in coverage when the number of layers is increased. To gain further insights into the morphology of these films, images at different scales are in Figs. 2**d and** 2**f**.

To analyze the morphology of 3 and 5-layer films, AFM images of different regions were taken. Figs. 2**g and** 2**h** collect the representative images of 3-layers (Fig. 2**g**) and 5-layers (Fig. 2**h**) films. The structural features obtained in the 3 L and 5 L films are quite similar and, although AFM is a local measurement, we have observed higher structures in the 5-layer film.

To analyze the quality of LS films, the crystallinity of perovskite films was analyzed by XRD. Fig. 3**a** presents the diffractograms of tree and five-layer LS films spread on Si/SiO_2 substrates.

The profiles present only diffraction peaks of (00 h), indicating that the layered perovskite is parallel to the film plane [37,44,61]. The lack of other reflections is due to a preferential orientation of the crystals along the (00 h) direction and the position of peaks is in good agreement with those observed in the diffractograms of 2D lead perovskites fabricated by LB methodology [37,44,61,62]. It is noticeable that the position of the peaks does not depend on the number of layers, suggesting that the incorporation of layers using this methodology does not influence the crystallinity of the films. This is likely due to the high control of the order achieved by the LS technique. The presence of eight periodic (00 h) peaks is indicative of the high purity of the layered perovskites [63]. It is important to note that the diffractograms of our perovskites show a greater number of reflections than those corresponding to perovskites obtained in a previous work by LB [61,64], and in perovskites synthesized in bulk [65–68], indicating higher crystallinity and consequently, higher quality. The crystallite size was calculated from the

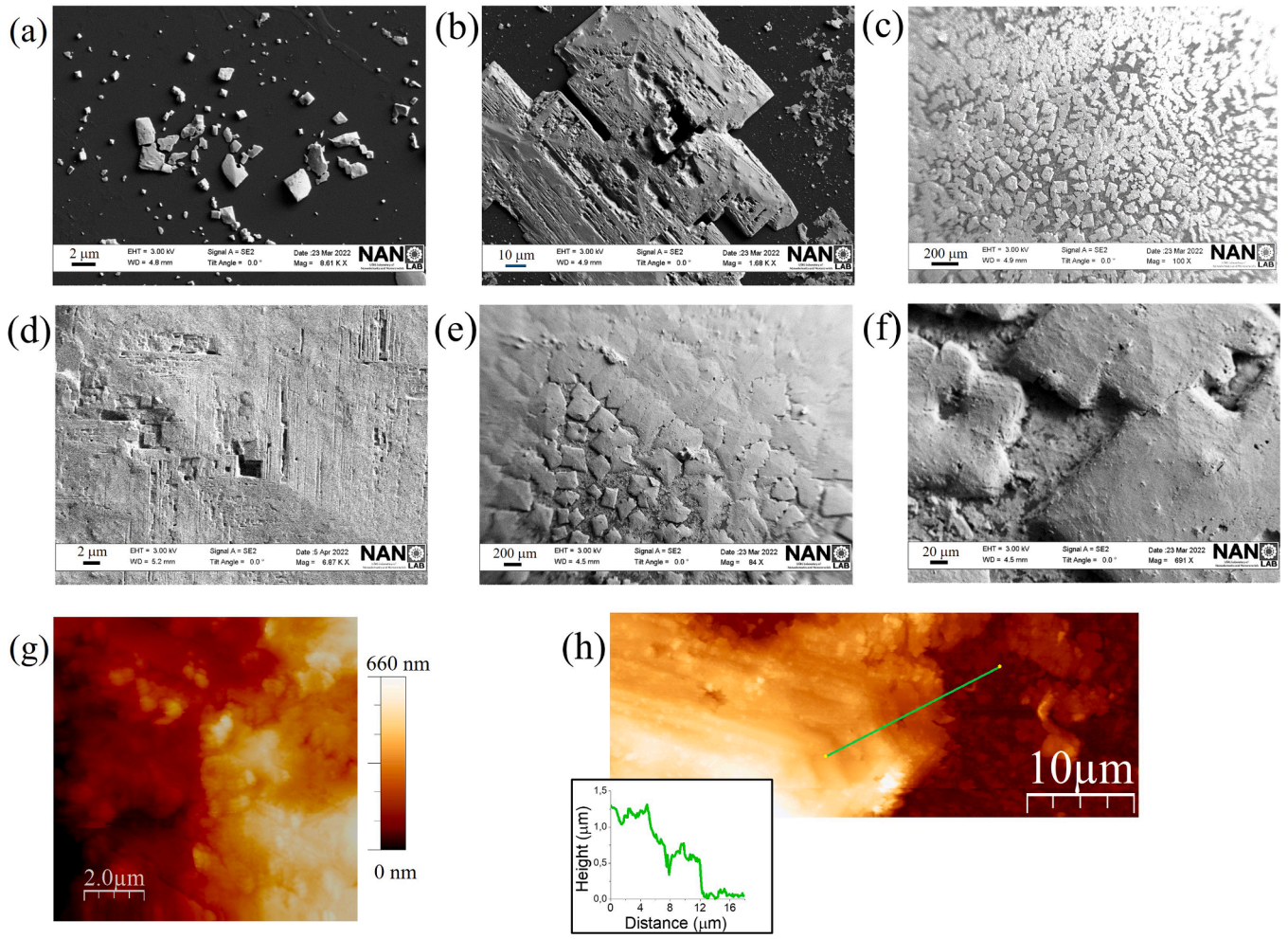

Fig. 2. SEM images of 2D bromide perovskites transferred from the air-liquid interface at 50 mN/m using the following methodologies: (a) Langmuir-Blodgett (1 layer); (b) Langmuir-Schaefer (1 layer); (c) and (d) Langmuir-Schaefer films of 3 layers; (e) and (f) Langmuir-Schaefer films of 5 layers. AFM images of perovskite films with: (g) 3-layers and (h) 5-layers.

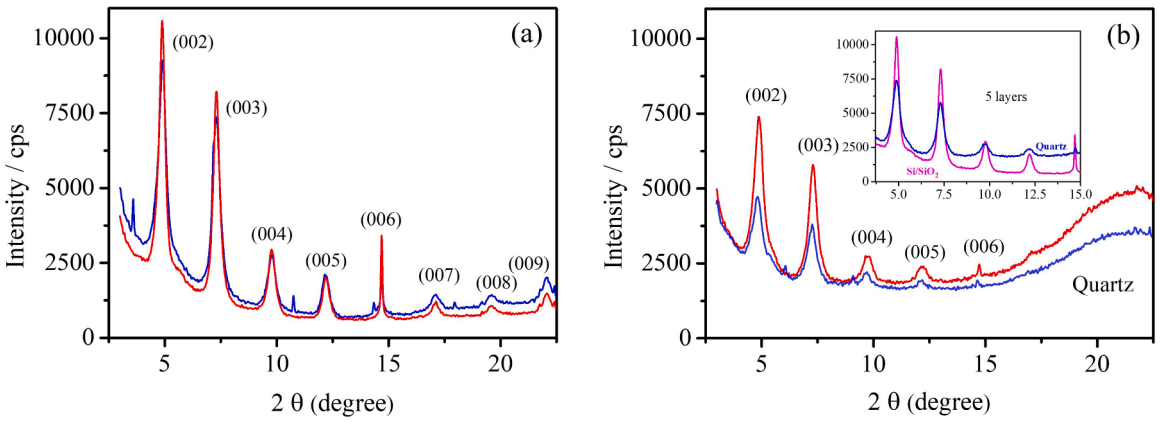

Fig. 3. X-ray diffractograms of 2D bromide perovskite LS films of 3-layers (blue line) and 5-layers (red line) spread on: (a) Si/SiO_2 and (b) quartz. For comparison inset in Fig. 3b collects diffractograms of a 5-layer film on silicon and quartz. The peaks are labeled with their corresponding diffraction planes.

Scherrer equation using the FWHM and Bragg angle values of the (002) peaks. The values found are (21.4 ± 0.8) nm and (25 ± 1) nm for 3- and 5-layer films, respectively. The value increases slightly as the number of layers increases. According to these values and considering the AFM analysis, it is possible to conclude that both 3- and 5- layer films are constituted by aggregate crystal [69].

From the position of the peaks and Bragg's law, the spacing of the layer (d) was calculated, with an average value of 3.62 nm. A comparison with the spacer length of the ODAB molecule (2.4 nm) [70] suggests that two octadecylammonium molecules are interdigitated and tilted with a large angle of around 48°. This behavior has previously been reported for a PbBr-based layered perovskites LB film using docosylammonium as organic layer [37].

The three-layer films diffraction pattern displays the emergence of additional peaks of extremely low intensity centered at 2θ = 3.598, 10.748, 14.336, 17.95 and 19.18°. The position of the peaks was used to calculate the layer spacing value of 4.1 nm. The emergence of these peaks in three-layer films seems to indicate some structural changes on the organic layers of perovskites, attributed to movements of the organic chains within the bilayer, which appear constrained with the addition of further layers. The low intensity of these new peaks indicates that these structural changes are not significant.

Since we have spread the organic perovskites on quartz to record the UV–vis absorption spectra, it is necessary to confirm that the structure of these films does not change when they are spread on quartz. With this aim, we have obtained the diffractograms of LS films of 3 and 5 layers on

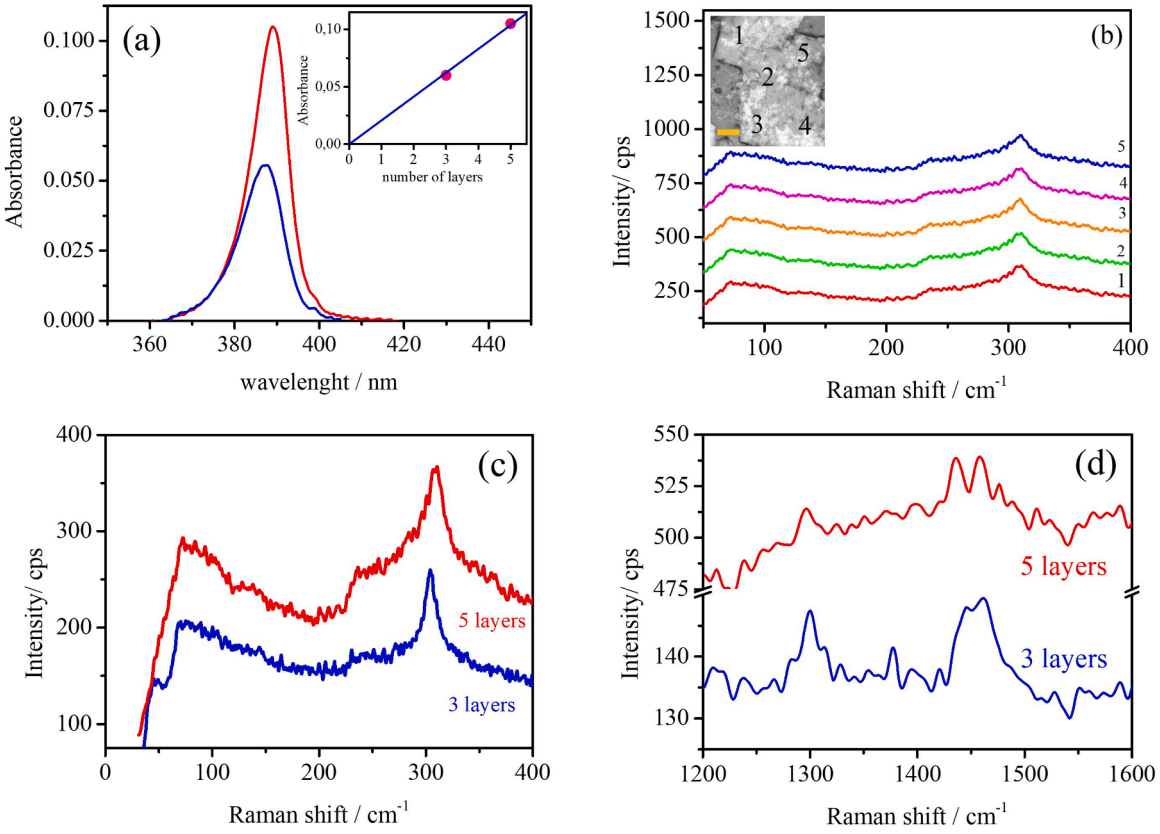

Fig. 4. (a) UV–vis spectra of 3-layer (blue line) and 5-layer (red line) films. (b) Raman spectra taken in different regions of a 5-layer film labeled in the inset image. The scale bar corresponds to 10 μm. (c) and (d) Averaged Raman spectra of 3-layer (blue line) and 5-layer (red line) perovskites LS films.

quartz, Fig. 3**b**. The figure shows the diffraction peaks of (00 h) from $h =$ 2 to 6. It was not possible to observe peaks corresponding to $h > 6$ due to the wide peak of quartz, which interferes with the perovskite peaks corresponding to $h > 6$. The position of the peaks does depend on the number of layers of the films, or the type of wafer used. The latter is shown in the inset of Fig. 3**b** which compares the diffractograms of 5-layer films deposited on Si/SiO_2 and quartz. Consequently, it can be concluded that the crystallinity of the perovskite LS films of 3 and 5 layers is comparable in the two solid wafers employed, quartz and Si/SiO_2.

The UV–Vis absorption spectra of the LS films with 3 and 5 layers are plotted in Fig. 4**a**.

The UV–vis spectra exhibit a maximum at 390 nm, which is independent of the number of layers spread and has been attributed to the exciton in the inorganic layer [71]. The position of the maximum is characteristic of perovskites constituted by a single layer of inorganic material [71] sandwiched between the organic layers. This means that our perovskite films fabricated by the LS technique contain just one layer of the inorganic moiety. From results obtained by XRD and UV–vis transmission measurements it was possible to conclude the composition of perovskite as $(C_{18}H_{37}\ NH_3)_2\ PbBr_3$.

The results presented here are consistent with recent theoretical calculations [72] which demonstrated that the optical properties of two-dimensional halide perovskites are mainly dominated by the electronic states of the inorganic metal-halide sheets. This is because the bandgap of the organic layers is larger (> 3 eV) than that of the inorganic layer.

The absorbance values were plotted as a function of the number of layers (inset of Fig. 4a). The graph shows a linear dependence between them, confirming the steady deposition of layered perovskite using the LS methodology. When the absorbance values of our LS films are compared with those obtained in a previous work [37] fabricated by the LB technique, we observe that the absorbance of our five-layer film is similar to that of 10 layers prepared by the LB method and using seven layers of cadmium arachidate covering the solid to increase the perovskite coverage [37]. This means that the LS methodology produces higher coverage than LB, even in non-modified solids.

The Raman spectra of three- and five-layer LS films on Si/SiO_2 are in Figs. 4**b-d**. Each Raman spectrum was recorded in at least five different zones of the films, and the results were found to be consistent, see Fig. 4**b**. Accordingly, the spectra plotted in Figs. 4**c and** 4**d** are the averages of these measurements. As can be seen in Fig. 4**c and** Fig. 4**d**, the spectra show peaks in two different regions, below 500 cm^{-1} and above 1200 cm^{-1}. The region between 500 and 1200 cm^{-1} has not been represented since it presents two very intense peaks centered at 520 and 900–1100 cm^{-1} assigned to one- and multi-phonon scattering respectively, from silicon substrate [73]. The high intensity of these peaks interferes with the spectra of perovskites in this spectral region. In the low wavenumbers, the Raman spectra present peaks below 100 cm^{-1}, which are assigned to the bending of the Br-Pb-Br bonds. Additionally, peaks between 100 and 250 cm^{-1} are observed as shoulders, and are assigned to the stretching of the Pb-Br bonds [74]. The peak centered at 310 cm^{-1} has been previously reported and was assigned to the torsional vibration of RNH_3^+ group [75,76]. Finally, bands at 1300, 1440 and 1460 cm^{-1} are assigned to C—N and C—H bending and C—H scissoring vibrations of the organic layer [77] of octadecylammonium bromide. Our Raman spectra demonstrate the presence of both, the organic and inorganic layers in the 2D bromide perovskites synthesized by the Langmuir-Schafer methodology and constituted additional evidence of the existence of 2D layered perovskites in our films.

4. Conclusions

In this work we report a novel synthesis of 2D-bromide perovskites at the interface based on the Langmuir-Schaefer technique. Our results demonstrate that this method represents an excellent procedure to obtain highly crystalline 2D-bromide perovskites. To our knowledge, this is the first time that the LS methodology has been proposed to prepare highly crystalline 2D-halide perovskites. Compared to other synthesis routes, it presents several advances. The LS method is a facile way to prepare 2D perovskite films. The perovskites prepared by LS have a crystallinity that exceeds the values achieved by other syntheses [73, 76–80]; and finally, the Langmuir Schaefer methodology is a versatile and scalable procedure that allows tuning the 2D perovskite structure according to applications, by modifying the organic molecules spread at the interface or the dopant ions dissolved in the aqueous subphase. Consequently, we strongly believe that this methodology opens new avenues for constructing layered perovskites with new functionalities that make their practical application possible.

CRediT authorship contribution statement

Rania Daoudi: Investigation. **David Durán:** Investigation. **David López-Díaz:** Writing – review & editing, Investigation. **Ana Pérez-Rodríguez:** Writing – review & editing, Investigation. **Maha Labani:** Investigation. **M. Dolores Merchán:** Writing – review & editing, Investigation. **M. Mercedes Velázquez:** Writing – review & editing, Writing – original draft, Investigation, Conceptualization.

Declaration of competing interest

The authors declare that they have no known competing financial interests or personal relationships that could have appeared to influence the work reported in this paper.

Acknowledgments

The work was financed by European Regional Development Fund, ERDF, and Junta de Castilla y León (SA106P23). A.P.R acknowledges financial support received by European Comission under the Marie Skłodowska-Curie-COFUND program, within the framework of the USAL4Excellence program (Grant Agreement No. 101034371). R.D and M.L. thank the Algerian government for their predoctoral scholarships. Authors thank the X-Ray diffraction service of the University of Salamanca for the XRD measurements.

Data availability

Data will be made available on request.

References

[1] S. Collavini, S.F. Völker, J.L. Delgado, understanding the outstanding power conversion efficiency of perovskite-based solar cells, 54(34) (2015) 9757–9759.
[2] G. Li, Y. Wang, L. Huang, W. Sun, Research progress of high-sensitivity perovskite photodetectors: a review of photodetectors: noise, structure, and materials, ACS Appl. Electr. Mater. 4 (4) (2022) 1485–1505.
[3] X.S. Zheng, S.M. Ma, Y.H. Zhang, M.Z. Wang, H.B. Fan, H.J. Feng, Enhancement of CsPbBr3 perovskite single-crystal photodetector performance via Zr Ion implantation, J. Phys. Chem. C 127 (25) (2023) 11780–11786.
[4] H. Hu, G. Niu, Z. Zheng, L. Xu, L. Liu, J. Tang, Perovskite semiconductors for ionizing radiation detection, 4(6) (2022) e12258.
[5] K.P. Goetz, Y. Vaynzof, The challenge of making the same device twice in perovskite photovoltaics, ACS. Energy Lett. 7 (5) (2022) 1750–1757.
[6] R. Szostak, A. de Souza Gonçalves, J.N. de Freitas, P.E. Marchezi, F.L. de Araújo, H. C.N. Tolentino, M.F. Toney, F. das Chagas Marques, A.F. Nogueira, Situ and operando characterizations of metal halide perovskite and solar cells: insights from lab-sized devices to upscaling processes, Chem. Rev. 123 (6) (2023) 3160–3236.
[7] A. Mandal, V. Hazra, S. Bhattacharyya, Perovskite nanostructure films for optoelectronics and photovoltaics, J. Phys. Chem. C 127 (25) (2023) 11767–11779.
[8] E. Kanao, T. Kubo, T. Naito, T. Matsumoto, T. Sano, M. Yan, K. Otsuka, Isotope Effects on Hydrogen Bonding and CH/CD−π Interaction, J. Phys. Chem. C 122 (26) (2018) 15026–15032.
[9] X. Hou, Y. Wang, H.K.H. Lee, R. Datt, N. Uslar Miano, D. Yan, M. Li, F. Zhu, B. Hou, W.C. Tsoi, Z. Li, Indoor application of emerging photovoltaics—Progress, challenges and perspectives, J. Mater. Chem. A 8 (41) (2020) 21503–21525.
[10] Y. Sun, L. Ge, L. Dai, C. Cho, J. Ferrer Orri, K. Ji, S.J. Zelewski, Y. Liu, A. J. Mirabelli, Y. Zhang, J.Y. Huang, Y. Wang, K. Gong, M.C. Lai, L. Zhang, D. Yang,

J. Lin, E.M. Tennyson, C. Ducati, S.D. Stranks, L.S. Cui, N.C. Greenham, Bright and stable perovskite light-emitting diodes in the near-infrared range, Nature 615 (7954) (2023) 830–835.
[11] W. Xu, Q. Hu, S. Bai, C. Bao, Y. Miao, Z. Yuan, T. Borzda, A.J. Barker, E. Tyukalova, Z. Hu, M. Kawecki, H. Wang, Z. Yan, X. Liu, X. Shi, K. Uvdal, M. Fahlman, W. Zhang, M. Duchamp, J.M. Liu, A. Petrozza, J. Wang, L.M. Liu, W. Huang, F. Gao, Rational molecular passivation for high-performance perovskite light-emitting diodes, Nat. Photonics. 13 (6) (2019) 418–424.
[12] M. Safdari, D. Phuyal, B. Philippe, P.H. Svensson, S.M. Butorin, K.O. Kvashnina, H. Rensmo, L. Kloo, J.M. Gardner, Impact of synthetic routes on the structural and physical properties of butyl-1,4-diammonium lead iodide semiconductors, J. Mater. Chem. A 5 (23) (2017) 11730–11738.
[13] C. Zhang, D.B. Kuang, W.Q. Wu, A review of diverse halide perovskite morphologies for efficient optoelectronic applications, 4(2) (2020) 1900662.
[14] B.w. Park, S.I. Seok, Intrinsic instability of inorganic–organic hybrid halide perovskite materials, 31(20) (2019) 1805337.
[15] Q. Dong, L. Lei, J. Mendes, F. So, Operational stability of perovskite light emitting diodes, J. Phys. 3 (1) (2020) 012002.
[16] P. Zhao, B.J. Kim, H.S. Jung, Passivation in perovskite solar cells: a review, Mater. Today Energy 7 (2018) 267–286.
[17] N. Jiang, G. Ma, D. Song, B. Qiao, Z. Liang, Z. Xu, S. Wageh, A. Al-Ghamdi, S. Zhao, Defects in lead halide perovskite light-emitting diodes under electric field: from behavior to passivation strategies, Nanoscale 16 (8) (2024) 3838–3880.
[18] W. Liu, Y. Lu, D. Wei, X. Huo, X. Huang, Y. Li, J. Meng, S. Zhao, B. Qiao, Z. Liang, Z. Xu, D. Song, Screening interface passivation materials intelligently through machine learning for highly efficient perovskite solar cells, J. Mater. Chem. A 10 (34) (2022) 17782–17789.
[19] D.S. Lee, J.H. Heo, J.K. Park, B.W. Kim, H.J. Lee, Y.M. Song, S.H. Im, Enhanced weak-light detection of perovskite photodetectors through perovskite/hole-transport material interface treatment, ACS. Appl. Mater. Interfaces. 13 (14) (2021) 16775–16783.
[20] M. Kim, G.H. Kim, T.K. Lee, I.W. Choi, H.W. Choi, Y. Jo, Y.J. Yoon, J.W. Kim, J. Lee, D. Huh, H. Lee, S.K. Kwak, J.Y. Kim, D.S. Kim, Methylammonium chloride induces intermediate phase stabilization for efficient perovskite solar cells, Joule 3 (9) (2019) 2179–2192.
[21] K.L. Svane, A.C. Forse, C.P. Grey, G. Kieslich, A.K. Cheetham, A. Walsh, K.T. Butler, How strong is the hydrogen bond in hybrid perovskites? J. Phys. Chem. Lett. 8 (24) (2017) 6154–6159.
[22] J. Hu, L. Yan, W. You, wo-dimensional organic–inorganic hybrid perovskites: a new platform for optoelectronic applications, T 30 (48) (2018) 1802041.
[23] M. Era, K. Maeda, T. Tsutsui, Self-organization approach to organic/inorganic quantum-well based on metal halide-based layer perovskite, Thin. Solid. Films. 331 (1) (1998) 285–290.
[24] Z. Chen, Q. Dong, Y. Liu, C. Bao, Y. Fang, Y. Lin, S. Tang, Q. Wang, X. Xiao, Y. Bai, Y. Deng, J. Huang, Thin single crystal perovskite solar cells to harvest below-bandgap light absorption, Nat. Commun. 8 (1) (2017) 1890.
[25] Y. Liu, Y. Zhang, X. Zhu, Z. Yang, W. Ke, J. Feng, X. Ren, K. Zhao, M. Liu, M.G. Kanatzidis, S. Liu, Inch-sized high-quality perovskite single crystals by suppressing phase segregation for light-powered integrated circuits, 7(7) (2021) eabc8844.
[26] D.B. Mitzi, Synthesis, crystal structure, and optical and thermal properties of (C4H9NH3)2MI4 (M = Ge, Sn, Pb), Chem. Mater. 8 (3) (1996) 791–800.
[27] C.C. Stoumpos, D.H. Cao, D.J. Clark, J. Young, J.M. Rondinelli, J.I. Jang, J. T. Hupp, M.G. Kanatzidis, Ruddlesden–popper hybrid lead iodide perovskite 2D homologous semiconductors, Chem. Mater. 28 (8) (2016) 2852–2867.
[28] Y. Gao, E. Shi, S. Deng, S.B. Shiring, J.M. Snaider, C. Liang, B. Yuan, R. Song, S. M. Janke, A. Liebman-Peláez, P. Yoo, M. Zeller, B.W. Boudouris, P. Liao, C. Zhu, V. Blum, Y. Yu, B.M. Savoie, L. Huang, L. Dou, Molecular engineering of organic–inorganic hybrid perovskites quantum wells, Nat. Chem. 11 (12) (2019) 1151–1157.
[29] K. Leng, I. Abdelwahab, I. Verzhbitskiy, M. Telychko, L. Chu, W. Fu, X. Chi, N. Guo, Z. Chen, Z. Chen, C. Zhang, Q.H. Xu, J. Lu, M. Chhowalla, G. Eda, K.P. Loh, Molecularly thin two-dimensional hybrid perovskites with tunable optoelectronic properties due to reversible surface relaxation, Nat. Mater. 17 (10) (2018) 908–914.
[30] J.Y. Park, Y.H. Lee, H. Kim, L. Dou, Two-dimensional perovskite heterostructures for single crystal semiconductor devices, J. Appl. Phys. 134 (6) (2023).
[31] A. Soultati, M. Tountas, K.K. Armadorou, A.R.b.M. Yusoff, M. Vasilopoulou, M. K. Nazeeruddin, Synthetic approaches for perovskite thin films and single-crystals, Energy Adv. 2 (8) (2023) 1075–1115.
[32] T. Zhang, L. Wang, L. Kong, C. Zhang, H. He, B. Wei, X. Yang, Halide perovskite based light-emitting diodes: a scaling up perspective, J. Mater. Chem. C 9 (24) (2021) 7532–7538.
[33] M. Mercedes Velázquez, Teresa Alejo, David López-Díaz, Beatriz Martín-García, María Dolores Merchán, Langmuir-blodgett methodology: a versatile technique to build 2D material films, in: P.K. Nayak (Ed.), Two-dimensional materials - synthesis, characterization and potential applications, 2016, pp. 21–42.
[34] T. Alejo, D. López-Díaz, B. Martín-García, M.D. Merchán, R. Sánchez-Hidalgo, M. M. Velázquez, 5 - Manufacturing ordered films of nanoparticles by Langmuir–Blodgett technique, in: M. Aliofkhazraei, N. Ali, M. Chipara, N. Bensaada Laidani, J.T.M. De Hosson (Eds.), Handbook of modern coating technologies, Elsevier, Amsterdam, 2021, pp. 121–138.
[35] R. Dong, T. Zhang, X. Feng, Interface-assisted synthesis of 2D materials: trend and challenges, Chem. Rev. 118 (13) (2018) 6189–6235.
[36] V.M. Kaganer, H. Möhwald, P. Dutta, Structure and phase transitions in Langmuir monolayers, Rev. Mod. Phys. 71 (3) (1999) 779–819.
[37] M. Era, S. Oka, PbBr-based layered perovskite film using the Langmuir–Blodgett technique, Thin. Solid. Films. 376 (1) (2000) 232–235.
[38] M. Era, T. Higashiuchi, K. Yaso, M. Kuramori, Y. Oishi, Formation of lead bromide-based layered perovskite monolayer having organic–inorganic quantum-well structure at air–water interface, Thin. Solid. Films. 499 (1) (2006) 49–53.
[39] M. Era, N. Takada, Squeezed-out technique to prepare high-quality PbBr-based layered perovskite langmuir–blodgett films applicable to cavity polariton devices, Langmuir. 35 (37) (2019) 12224–12228.
[40] G.G. Roberts, Langmuir-blodgett films, Springer Science, Oxford U.K., 1990.
[41] K. Ariga, Don't forget langmuir–blodgett films 2020: interfacial nanoarchitectonics with molecules, materials, and living objects, Langmuir. 36 (26) (2020) 7158–7180.
[42] O.N. Oliveira Jr., L. Caseli, K. Ariga, The past and the future of langmuir and langmuir–blodgett films, Chem. Rev. 122 (6) (2022) 6459–6513.
[43] T. Alejo, P.M.R. Paulo, M.D. Merchán, E. Garcia-Fernandez, S.M.B. Costa, M. M. Velázquez, Influence of 3D aggregation on the photoluminescence dynamics of CdSe quantum dot films, J. Lumin. 183 (2017) 113–120.
[44] M. Era, Y. Shironita, K. Soda, Lead bromide-based layered perovskite Langmuir–Blodgett films having π-conjugated molecules as organic layer prepared by using squeezed out technique, Jpn. J. Appl. Phys. 57 (3S2) (2018) 03EG07.
[45] Y. Oishi, E. Tsukamoto, M. Shimoda, T. Takamuku, T. Narita, M. Era, A novel preparation method of lead-based layered perovskite Langmuir films with a negligible amount of PbBr2, New J. Chem. 37 (3) (2013) 568–570.
[46] I. Langmuir, V.J. Schaefer, Activities of urease and pepsin monolayers, J. Am. Chem. Soc. 60 (6) (1938) 1351–1360.
[47] M. Bodik, O. Maxian, J. Hagara, P. Nadazdy, M. Jergel, E. Majkova, P. Siffalovic, Langmuir–Scheaffer technique as a method for controlled alignment of 1D materials, Langmuir. 36 (16) (2020) 4540–4547.
[48] M. Bodik, P. Siffalovic, P. Nadazdy, M. Benkovicova, Z. Markovic, J. Chlpik, J. Cirak, M. Kotlar, M. Micusik, M. Jergel, E. Majkova, On the formation of hydrophobic carbon quantum dots Langmuir films and their transfer onto solid substrates, Diam. Relat. Mater. 83 (2018) 170–176.
[49] A.R. Tao, J. Huang, P. Yang, Langmuir-blodgettry of nanocrystals and nanowires, Acc. Chem. Res. 41 (12) (2008) 1662–1673.
[50] D. López-Diaz, C. Merino, M. Velázquez, Modulating the optoelectronic properties of silver nanowires films: effect of capping agent and deposition technique, Materials. 8 (11) (2015) 5405.
[51] M. Lafuente, S. Ruiz-Rincón, R. Mallada, P. Cea, M.Pilar Pina, Towards the reproducible fabrication of homogeneous SERS substrates by Langmuir-Schaefer technique: a low cost and scalable approach for practical SERS based sensing applications, Appl. Surf. Sci. 506 (2020) 144663.
[52] M. Wang, B. Li, J. Yuan, F. Huang, G. Cao, J. Tian, Repairing defects of halide perovskite films to enhance photovoltaic performance, ACS. Appl. Mater. Interfaces. 10 (43) (2018) 37005–37013.
[53] S. Shao, J. Dong, H. Duim, G.H. ten Brink, G.R. Blake, G. Portale, M.A. Loi, Enhancing the crystallinity and perfecting the orientation of formamidinium tin iodide for highly efficient Sn-based perovskite solar cells, Nano Energy 60 (2019) 810–816.
[54] I. Koutselas, P. Bampoulis, E. Maratou, T. Evagelinou, G. Pagona, G. C. Papavassiliou, Some unconventional organic−inorganic hybrid low-dimensional semiconductors and related light-emitting devices, J. Phys. Chem. C 115 (17) (2011) 8475–8483.
[55] B. Luo, Y.C. Pu, Y. Yang, S.A. Lindley, G. Abdelmageed, H. Ashry, Y. Li, X. Li, J. Z. Zhang, Synthesis, optical properties, and exciton dynamics of organolead bromide perovskite nanocrystals, J. Physic. Chem. C 119 (47) (2015) 26672–26682.
[56] J.T.R. Davies, Interfacial Phenomena, E.K., Academic Press, New York, 1963.
[57] L. Xu, X. Chen, L. Wang, Z. Sui, J. Zhao, B. Zhu, Formation of lead sulfide nanoparticles via Langmuir–Blodgett technique, Physicochem. Eng. Asp. 257-258 (2005) 457–460.
[58] Z. Khattari, U. Langer, S. Aliaskarisohi, A. Ray, T.M. Fischer, Effects of soluble surfactants on the Langmuir monolayers compressibility: a comparative study using interfacial isotherms and fluorescence microscopy, Mater. Sci. Eng. 31 (8) (2011) 1711–1715.
[59] M. Dolores Merchán, N. Pawar, A. Santamaria, R. Sánchez-Fernández, O. Konovalov, A. Maestro, M.Mercedes Velázquez, Structure of graphene oxide-phospholipid monolayers: a grazing incidence X-ray diffraction and neutron and X-ray reflectivity study, J. Colloid. Interface Sci. 655 (2024) 664–675.
[60] F. Sahli, J. Werner, B.A. Kamino, M. Bräuninger, R. Monnard, B. Paviet-Salomon, L. Barraud, L. Ding, J.J. Diaz Leon, D. Sacchetto, G. Cattaneo, M. Despeisse, M. Boccard, S. Nicolay, Q. Jeangros, B. Niesen, C. Ballif, Fully textured monolithic perovskite/silicon tandem solar cells with 25.2% power conversion efficiency, Nat. Mater. 17 (9) (2018) 820–826.
[61] M. Era, A. Shimizu, PBI-based layered perovskite organic-inorganic superlattice film by the langmuir-blodgett technique, Mole. Cryst. Liquid Cryst. Sci. Techn.. Sect. A. Mol. Cryst. Liq. Crys. 370 (1) (2001) 215–218.
[62] N. Akhtar, A.O. Polyakov, A. Aqeel, P. Gordiichuk, G.R. Blake, J. Baas, H. Amenitsch, A. Herrmann, P. Rudolf, T.T.M. Palstra, Self-Assem. Ferromagn. Org.–Inorg. Perovskite-Like Films, 10 (23) (2014) 4912–4919.
[63] S. Ghimire, C. Klinke, Two-dimensional halide perovskites: synthesis, optoelectronic properties, stability, and applications, Nanoscale 13 (29) (2021) 12394–12422.
[64] M. Era, Y. Komatsu, N. Sakamoto, Enhancement of exciton emission in lead halide-based layered perovskites by cation mixing, J. Nanosci. Nanotechnol. 16 (4) (2016) 3338–3342.

[65] R. Hamaguchi, M. Yoshizawa-Fujita, T. Miyasaka, H. Kunugita, K. Ema, Y. Takeoka, M. Rikukawa, Formamidine and cesium-based quasi-two-dimensional perovskites as photovoltaic absorbers, Chem. Commun. 53 (31) (2017) 4366–4369.
[66] Y. Hu, L.M. Spies, D. Alonso-Álvarez, P. Mocherla, H. Jones, J. Hanisch, T. Bein, P. R.F. Barnes, P. Docampo, Identifying and controlling phase purity in 2D hybrid perovskite thin films, J. Mater. Chem. A 6 (44) (2018) 22215–22225.
[67] B. Chen, K. Meng, Z. Qiao, Y. Zhai, R. Yu, Z. Fang, P. Yan, M. Xiao, L. Pan, L. Zheng, K. Cao, G. Chen, Surface crystallization modulation toward highly-oriented and phase-pure 2D perovskite solar, Cells 36 (21) (2024) 2312054.
[68] A.S. Tutantsev, E.I. Marchenko, N.N. Udalova, S.A. Fateev, E.A. Goodilin, A. B. Tarasov, Structural disorder in layered hybrid halide perovskites: types of stacking faults, influence on optical properties and their suppression by crystallization engineering, Nanomaterials. (Basel) 11 (12) (2021).
[69] L. Atourki, E. Vega, B. Marí, M. Mollar, H. Ait Ahsaine, K. Bouabid, A. Ihlal, Role of the chemical substitution on the structural and luminescence properties of the mixed halide perovskite thin MAPbI3−xBrx (0≤x≤1) films, Appl. Surf. Sci. 371 (2016) 112–117.
[70] C. Tanford, The hydrophobic effect: formation of micelles and biological membranes, 2nd Edition, Wyley-Interscience pub, New York, 1980.
[71] Y. Takeoka, K. Asai, M. Rikukawa, K. Sanui, Systematic studies on chain lengths, halide species, and well thicknesses for lead halide layered perovskite thin films, Bull. Chem. Soc. Jpn. 79 (10) (2006) 1607–1613.
[72] S. Wang, Z. Chen, G. Zhao, F. Wang, Quantum confinement effect on the electronic and optical properties of two-dimensional halide perovskites, Comput. Mater. Sci. 230 (2023) 112524.
[73] P.A. Temple, C.E. Hathaway, Multiphonon raman spectrum of silicon, Phys. Rev. B 7 (8) (1973) 3685–3697.
[74] L. Mao, P. Guo, M. Kepenekian, I. Hadar, C. Katan, J. Even, R.D. Schaller, C. C. Stoumpos, M.G. Kanatzidis, Structural diversity in white-light-emitting hybrid lead bromide perovskites, J. Am. Chem. Soc. 140 (40) (2018) 13078–13088.
[75] A.M.A. Leguy, A.R. Goñi, J.M. Frost, J. Skelton, F. Brivio, X. Rodríguez-Martínez, O.J. Weber, A. Pallipurath, M.I. Alonso, M. Campoy-Quiles, M.T. Weller, J. Nelson, A. Walsh, P.R.F. Barnes, Dynamic disorder, phonon lifetimes, and the assignment of modes to the vibrational spectra of methylammonium lead halide perovskites, Phys. Chem. Chemic. Phys. 18 (39) (2016) 27051–27066.
[76] R.G. Niemann, A.G. Kontos, D. Palles, E.I. Kamitsos, A. Kaltzoglou, F. Brivio, P. Falaras, P.J. Cameron, Halogen effects on ordering and bonding of CH3NH3+ in CH3NH3PbX3 (X = Cl, Br, I) hybrid perovskites: a vibrational spectroscopic study, J. Physic. Chem. C 120 (5) (2016) 2509–2519.
[77] Y. Xi, Z. Ding, H. He, R.L. Frost, Infrared spectroscopy of organoclays synthesized with the surfactant octadecyltrimethylammonium bromide, Mole. Biomol. Spectrosc. 61 (3) (2005) 515–525.